

Geophysical Research Letters

RESEARCH LETTER

10.1029/2019GL083057

Key Points:

- MMS observed 11-min-long lobe reconnection surge near the separatrix during fast poleward electrojet expansion in the conjugate ionosphere
- Intense hard electron precipitation near the footpoint of the neutral line and dipolarized fieldlines in the interior of auroral bulge are confirmed
- Direct link and consistency of poleward auroral expansion and reconnection rates are demonstrated

Supporting Information:

- Supporting Information S1

Correspondence to:

V. A. Sergeev,
victor@geo.phys.spbu.ru

Citation:

Sergeev, V. A., Apatenkov, S. V., Nakamura, R., Baumjohann, W., Khotyaintsev, Y. V., Kauristie, K., et al. (2019). Substorm-related near-Earth reconnection surge: Combining telescopic and microscopic views. *Geophysical Research Letters*, 46, 6239–6247. <https://doi.org/10.1029/2019GL083057>












Received 29 MAR 2019

Accepted 4 JUN 2019

Accepted article online 7 JUN 2019

Published online 24 JUN 2019

Substorm-Related Near-Earth Reconnection Surge: Combining Telescopic and Microscopic Views

V. A. Sergeev¹ , S. V. Apatenkov¹, R. Nakamura² , W. Baumjohann² , Y. V. Khotyaintsev³ , K. Kauristie⁴ , M. van de Kamp⁴, J. L. Burch⁵ , R. E. Ergun⁶ , P.-A. Lindqvist⁷ , R. Torbert⁸ , C. T. Russell⁹ , and B. L. Giles¹⁰ 

¹Earth's Physics Department, St. Petersburg State University, St. Petersburg, Russia, ²Space Research Institute, Austrian Academy of Sciences, Graz, Austria, ³Swedish Institute of Space Physics, Uppsala, Sweden, ⁴Finnish Meteorological Institute, Helsinki, Finland, ⁵Southwest Research Institute, San Antonio, TX, USA, ⁶Laboratory for Atmospheric and Space Physics, University of Colorado Boulder, Boulder, CO, USA, ⁷Department of Space and Plasma Physics, KTH Royal Institute of Technology, Stockholm, Sweden, ⁸Space Science Center, University of New Hampshire, Durham, NH, USA, ⁹IGPP/EPSS, University of California, Los Angeles, CA, USA, ¹⁰NASA Goddard Space Flight Center, Greenbelt, MD, USA

Abstract A strong ~11-min-long surge of the lobe reconnection was observed during a substorm on the tailward side of the near-Earth neutral line. In the southern lobe near the reconnection separatrix the MMS spacecraft observed short-duration earthward electron beams providing the local Hall current, tailward propagating Alfvén wave (AW) bursts with Poynting flux up to 10^{-4} W/m², and large-amplitude *E* field spikes (e-holes) and low hybrid waves. The reconnection surge was accompanied by substorm current wedge formation and fast poleward expansion of auroral bulge-related westward electrojet in the conjugate ionosphere. During its meridional crossing above the expanding bulge the Metop-2 spacecraft observed an intense energetic precipitation spike near the expected X line foot point and confirmed the dipolarized character of magnetic field lines inside of the bulge. Globally the observed average reconnection rate ($\langle E_y \rangle \sim 3.3$ mV/m) was sufficient to produce the magnetic flux increase in the bulge, associated with observed fast poleward expansion (about 6° latitude in 5 min).

Plain Language Summary Although magnetic reconnection in the magnetotail has been proposed to be the core process for the strong global magnetospheric reconfiguration and for huge particle acceleration during magnetospheric substorms, this association is mostly based on indirect evidence, because reconnection intermittently activates in different parts of the tail current sheet, and it is difficult to monitor its location and intensity variations based on direct spacecraft observations. On 28 July 2017 the MMS spacecraft succeeded in staying in the magnetotail near the active reconnection separatrix for a relatively long time during the surge of reconnection. At the same time the electric currents were enhanced and moved poleward in the magnetically conjugate part of the ionosphere, indicating configurational changes in the magnetotail. At the same minute the Metop-2 spacecraft in low-Earth orbit passed above this region and detected precipitating electrons of different energies as well as their distribution in the loss cone, which yielded conclusions about the strength of the equatorial magnetic field in the reconnected flux tubes. This unprecedented combination of conjugate observations allows us to confirm directly the important global consequences of an intense near-Earth reconnection event, which have been suggested in the near-Earth neutral line substorm scenario but could not be previously observed together in the same event.

1. Introduction

Magnetic reconnection is a multiscale process whose basic kinetic scales are as small as the electron and ion gyro/inertial scales (tens to hundreds of kilometers in the magnetospheric plasma). Exploration of these microscopic aspects is the primary goal of the current MMS mission (Burch et al., 2015). However, the large community interest in magnetic reconnection comes from its highly important macroscopic consequences, which are supposed to include such explosive phenomena in the plasma universe as magnetospheric substorms, solar flares, and coronal mass ejections (which severely influence the space weather) and others. Therefore, an important aspect of the magnetospheric MMS project can also be to improve our quantitative understanding of the coupling between properly monitored microscale reconnection phenomena and their macroscale consequences, particularly, magnetospheric substorms.

The role of reconnection in magnetospheric substorms is a traditional topic, which stimulated a lot of research during the first decades of magnetospheric studies. A summary of spacecraft and ground-based observations complemented by global auroral imaging resulted in a widely known reconnection-based scenario for substorms, known as the near-Earth neutral line (NENL) model (see, e.g., Hones, 1984; Baker et al., 1996). It provided a framework to organize diverse observed substorm-related phenomena and to interpret the basic large-scale substorm-related changes in the magnetotail known thus far, and it even helped to predict some new phenomena such as the spectacular tailward moving plasmoids in the distant magnetotail. Since then, in spite of significant development of observational systems and global simulation capabilities, our understanding of magnetotail dynamics and its relationship to the tail reconnection still continues to be mostly qualitative and primarily based on indirect evidence and interpretations, with a much smaller amount of direct quantitative comparisons available so far. Major limitations include difficulty in monitoring and quantifying the large-scale dynamical changes in the tail and, especially, due to very limited possibilities to monitor the reconnection location and reconnection rate in the magnetotail.

One reason for the lack of quantitative comparisons is that the reconnection process itself (and substorm activations in general) is a multiscale process with highly complicated spatiotemporal dynamics (Paschmann et al., 2013). The reconnection lines (XNLs, for brevity) emerge and develop sporadically for a short time in different localized regions of thin current sheet and then migrate to or reappear in the new regions. Because of such irregular intermittent appearances, it is usually very difficult to observe the actual reconnection rate by magnetospheric spacecraft for a sufficiently long time. At the same time, the large-scale consequences of interest are formed by integral effects of the reconnection process. Therefore, short sporadic appearances of reconnection makes it difficult to establish the observation-based quantitative relationships related to the macroscopic effects. To some extent, remote observations of magnetic flux transported in the fast flow burst channels created by reconnection can help to characterize reconnection in operation, but they do not provide precise diagnostics, because the observed flows result from complicated interaction of reconnection outflow with inhomogeneous plasma sheet, including interchange motions of plasma tubes having different properties. Also, because sporadic reconnection is localized across the tail and the localized outflow develops basically within the magnetic field (meridional) planes in the tail, the quantitative comparison of the cause and the effect should be done in the same magnetic meridional plane, which is rarely possible with a sparse coverage of existing magnetospheric spacecraft.

Modelling capabilities have greatly improved during the last decade, especially global magnetohydrodynamic (MHD) simulations, which allow us to simulate global consequences of magnetotail reconnection under realistic variable solar wind inputs. Particularly, the high-resolution global simulations (done both with and without coupling to the drift physics equations in the inner tail region, e.g., Pembroke et al., 2012, and Wiltberger et al., 2015, correspondingly) provide a nice illustration of complicated localized sporadic activities which cooperate to form the enhanced plasma sheet convection, dipolarization, and substorm current wedge (see also Birn & Hesse, 2013). Unfortunately global simulations do not properly include kinetic physics which is central for reconnection, and different MHD model realizations provide drastically different global dynamical responses when tested for similar input conditions (Gordeev et al., 2017). Therefore, while global MHD simulations continue providing perspective, they cannot yet provide an absolute answer (the ground truth) regarding global magnetotail dynamics.

Returning to observations, much better chances of directly linking reconnection and its consequences exist in the case where three conditions are fulfilled together, namely, (a) the reconnection rate is large and continues for a longer time (i.e., 10 min or so), while the XNL location does not change much; (b) monitoring the consequences is provided in the same meridional plane where reconnection is directly observed; and (c) global information is available to place the reconnection event into the global activity context, both temporally and spatially. As previously noticed by Baker et al. (2016), in such studies it is essential to combine a detailed (microscopic) view of the core phenomenon (here, to identify and quantify the parameters of the reconnection process) with a global (telescopic) view of various associated phenomena.

The three conditions mentioned above seem to fulfill our event study of a moderate substorm event, in which significant enhancement of the reconnection rate in the near-tail region continued for more than 10 min. This time, MMS spacecraft probed the reconnection in the tail lobe near the separatrix, which is a favorable place for measurement of the reconnection rate. Using ground-based and low-altitude spacecraft

observations near the magnetic meridional plane where the reconnection was in progress, we can follow the activation and poleward expansion of substorm-related westward electrojet. In this way we relate the expansion rate with the reconnection rate, identify the hard and intense precipitation structure near the expected XNL foot point in the ionosphere, and identify the foot points of dipolarized magnetic flux tubes which form the auroral bulge.

2. Observations

After 1820 UT on 28 July 2017 an isolated substorm was initiated by the southward interplanetary magnetic field (IMF) turning. Its expansion phase onset was identified at about 1903 UT by the commencement of the global Pi2 pulsations and the midlatitude magnetic bays (signatures of substorm current wedge, SCW; Figure 1b). At nearly this time, the westward auroral electrojet (AEJ) was enhanced in the nightside auroral zone (Figure 1a). The midlatitude bay relaxed after ~ 1920 UT, and it almost recovered when a new bay-like perturbation and global Pi2 commenced at about 1942 UT. Whereas the first SCW activation developed in the midnight, that is, 22.5–01.5 magnetic local time (MLT) sector (see, e.g., the change of the ΔY perturbation sign that occurred at around AMS station), the second SCW activation occupied the premidnight sector at 19–23.5 MLT. The largest ΔX and $\Delta Y \sim 0$ were recorded at Crozet Isl (CZT) located at about Scandinavian magnetic meridian, which is magnetically conjugate to MMS. Impulsive activation of the westward AEJ and its poleward expansion after 1942 UT were comprehensively observed at the Scandinavian meridian (see records of JAN and BJN stations in Figure 1a); they will be analyzed in more detail below. Between 19 and 20 UT, there was nothing significant in the solar wind. According to the OMNIWeb database, the solar wind flow pressure varied slightly at around 2 nPa (not shown), and IMF B_Z was persistently southward at around $-2 \dots -3$ nT level (Figure 1c).

The Pi2 + SCW activations were accompanied by an enhanced E_y component at MMS, indicating the enhanced dissipation in the magnetotail (Figure 1d). This time MMS was $0.5 R_E$ southward of the nominal tail current sheet center, and the local normal to the neutral sheet surface was very close to Z_{GSE} (see the supporting information Figure S1). All MMS spacecraft operated in the fast survey mode, MMS3 was at the top, and MMS4 was at the bottom of MMS formation, being separated by ~ 20 km. Staying in the central plasma sheet ($P_p/P_B \sim 1$) at the onset (1903 UT), it observed the modest E_y (in average ~ 1 mV/m) and southward B_Z variation, suggestive of the reconnection initiated closer to the Earth. However, no fast tailward ion outflow has been recorded. Soon after, the observations indicated plasma/current sheet thinning (see bottom panel in Figure 1d), leaving MMS in the southern lobe. Interestingly, during that part of expansion phase between 1915 and 1940 UT, the B field magnitude was continuously increasing at MMS (see B_x in Figure d), indicating the growth of the tail electric current in this MLT sector.

Manifestations of the second substorm activation were dramatic. The MMS spacecraft stayed in the lobe close to the plasma sheet boundary and, starting from 1940:30 UT, they observed a dramatic enhancement of the E_y component, indicating that magnetic flux tubes flow into the plasma sheet at a very high rate for about 11 min. The strongest inflow rates, above 3 mV/m, were observed between 1941 and 1947 UT. This was observed together with another dramatic signature, a fast, steady decrease of the lobe magnetic field magnitude, signaling significant loss of (reconnected) magnetic flux during this episode. In combination, these two signatures classify this episode as an intense reconnection surge. We first analyze the details of MMS observations to confirm and elaborate this interpretation, to locate the MMS spacecraft against the X-type XNL, and to quickly discuss how the magnetic separatrix looks in observations.

Most of the time shown in Figure 2, MMS spent in the southern lobe as indicated by recordings of ~ 100 -eV polar rain electrons (Figure 2c) and by a spectacular trace of the cold ions in Figure 2a showing the lobe population, which is known from previous studies (e.g., Varsani et al., 2017). As in those previous papers, at the top of spectrogram (a) we overplotted the trace of kinetic energy due to the proton convective transport ($Ep = m_p VE^2/2$, $\mathbf{VE} = (\mathbf{E} \times \mathbf{B})/B^2$). Its good agreement with omnidirectional spectrogram indicates that the cold ions were mostly protons, and that VE quantitatively provided a robust estimate of the convection. During this episode there was no indication of energetic ion beams so that the spacecraft definitely did not enter into the proton plasma sheet boundary layer in this episode. At the same time there were definitely three 10- to 20-s-long intense electron beams. The beams were about a few to

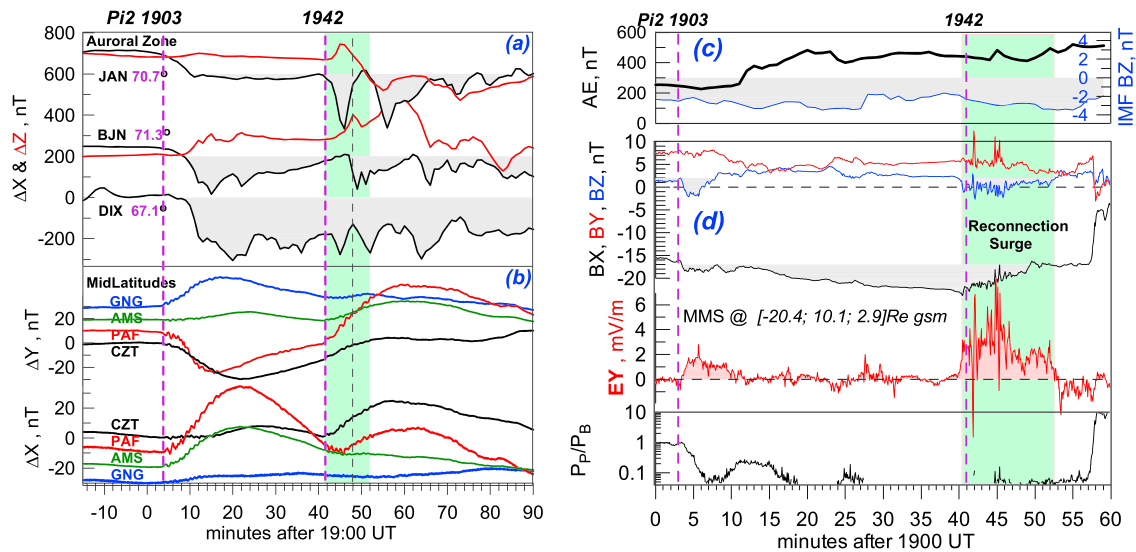


Figure 1. Overview of activity during a substorm on 28 July 2017. (a, b). Magnetograms of auroral zone stations at 1-min resolution (a) and of midlatitude stations at 1-s resolution (b); at 19 UT the magnetic local times of stations were 2.8 hr (GNG), 0.6 hr (AMS), 23.5 hr (PAF), and 22.5 hr (CZT). (c) Interplanetary magnetic field B_Z (blue line) and AE index (black line); (d) magnetic and electric field geocentric solar equatorial components and plasma beta observed at MMS3 spacecraft.

several kiloelectron volts in energy, and the ~ 100 -eV polar rain was completely replaced by these beams (Figure 2c) suggesting its possible acceleration by the field-aligned E field. The beams were highly collimated antiparallel to B , moving in an earthward direction (Figure 2b).

A number of spectacular E and B field phenomena were registered during the convection surge after 1940.5 UT. The appearance of AWs is visually seen as a component-by-component anticorrelation between magnetic field (Figure 2d) and convection VE (Figure 2e) perturbations. (see supporting information Figure S2 for more detailed correlation plots). The anticorrelation corresponds to outward AW propagation in the southern lobe. We also computed the Poynting flux using 1-s average values of perturbations after subtracting the trend (defined using 1-min average sliding window). It showed a predominantly positive (means, outward) field-aligned flux S_{\parallel} (Figure 2f) which is enhanced up to 10^{-4} W/m² during the electron beams. The amplitude of electrostatic waves also greatly increased during these brief beam encounters (Figure 2g), with ΔE peak fluctuation magnitude in 32-Hz data reaching as much as ~ 100 mV/m; intense fluctuations were interpreted as low hybrid waves with superposed spikes resembling the electron holes.

Concerning the location of the XNL in this episode, the bulk of evidence (negative B_Z variation, outward AW propagation, and outward Poynting flux) tells us that MMS made measurements on the tailward side of XNL being at $X < -20 R_E$ (NENL case). Throughout the whole event B_Z variation (emphasized by shading in Figures 1d and 2d) was negative as compared to its stable preceding level of $\sim +1 \dots 2$ nT (which corresponds to the B_Z offset due to neutral sheet tilt, Figure S1); thus indicating no evidence of tailward retreat of the active XNL. The collimated earthward electron beam (toward the XNL) could then be the lobeward part of the Hall electric circuit (\mathbf{j} directed tailward) which creates duskward (positive) Hall BY spikes. Thus, the morphology of all these manifestations is fully consistent with the reconnection-based picture if the observations were made in the proximity of the magnetic separatrix, without entering into the reconnection exhaust. Taking into account that in particle-in-cell (PIC) simulations the inward e-beam is most pronounced at roughly 20 ion inertial lengths from XNL (e.g., Hesse et al., 2016, Figure 2), we can estimate MMS being at a distance of a few R_E from the reconnection site.

We look at the global consequences by examining low-altitude and ionospheric observations (Figure 3). This time, the electrojet dynamics were monitored by the IMAGE magnetometer array in Fennoscandia (Figure 3a), which occupied the area between the meridians 21 and 22 hr MLT, where the MMS foot point is approximately mapped to and where the POES Metop-2 low-altitude ($h \sim 850$ km) spacecraft passed during the reconnection surge (see a map in Figure 3b). (We caution that the standard model cannot exactly

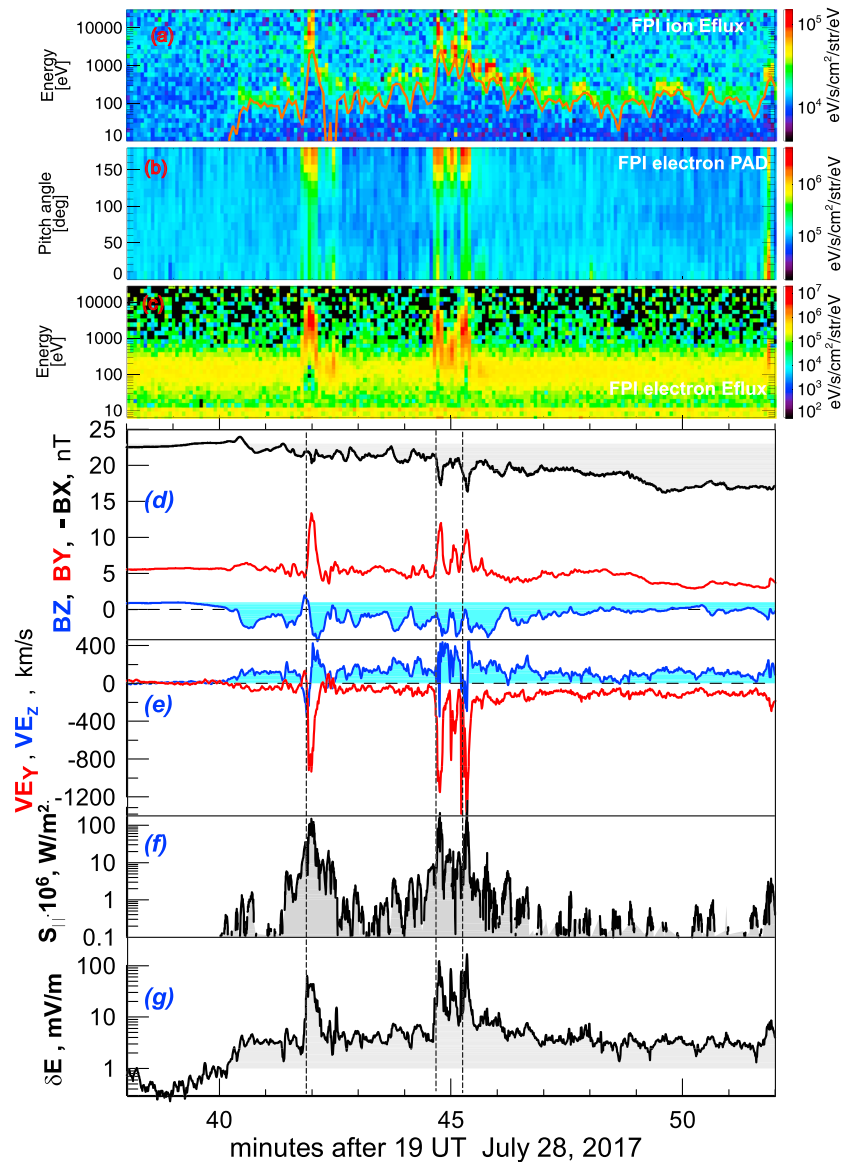


Figure 2. Observations of reconnection surge at MMS3: Omnidirectional Fast Plasma Investigation (FPI) ion spectrogram (a); pitch-angle distribution of 0.2- to 2-keV electrons (b); spectrogram for antiparallel electrons (c); magnetic field components (d); convection flow $\mathbf{VE} = (\mathbf{E} \times \mathbf{B})/B^2$ components at 1-s resolution (e); field-aligned component of Poynting flux $(\delta\mathbf{E} \times \delta\mathbf{B}) \cdot \langle \mathbf{B} \rangle / \langle B \rangle \mu_0$ (f); peak δE -field changes within 1-s time intervals (g).

predict the latitude of the MMS foot point, which varies with the substorm-related changes of the tail current). The westward electrojet (blue color) slowly relaxed after 1935 UT, and by 1942 UT, its poleward edge descended down to 70° GeoLat (about 67° altitude-adjusted corrected geomagnetic (AACG) latitude at 20° geographic meridian (GG)). After 1943 UT it showed the intensity variations and poleward expansion, and by 1949 UT the poleward edge of westward current reached its highest latitude 76° (about 73° AACG) latitude). It may be of interest that one may discern two to three activations (leap elements) during this poleward expansion. One more, a detached high-latitude activation of westward electrojet, was observed at 2001 UT, closely following the fast plasma sheet expansion observed by MMS at 1958 UT (Figure 3d).

According to Figures 3b and 3c, Metop-2 (M02) passed from south to north above the expanding electrojet between 1944 and 1948 UT, allowing us to monitor at a 2-s time resolution the particle precipitation resulting from the reconnection surge. After 1947:31 M02 was in the polar cap, as indicated by the low level of both

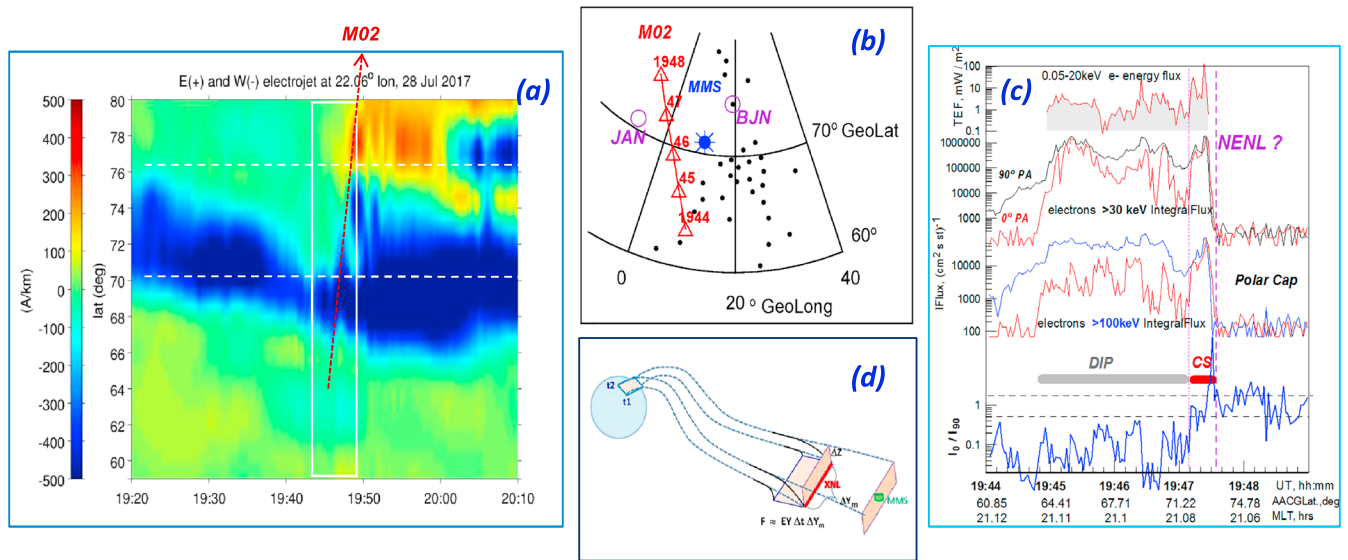


Figure 3. (a) Meridional distributions of equivalent east-west currents at Scandinavian meridian (blue, westward electrojet; yellow, eastward current). (b) Map showing distribution of International Monitor for Auroral Geomagnetic Effects (IMAGE) magnetometers (dots), Metop-2 (M02) spacecraft trajectory (red triangles), and ionospheric foot point of MMS along magnetic field line of TA15 model (blue star). (c) Observations of electron precipitation and loss-cone filling ratio of energetic electrons for >100 keV (blue line on bottom) on board Metop-2 spacecraft; corrected geomagnetic (AACG) coordinates are given for spacecraft mapped to 120-km altitude. (d) Scheme illustrating the comparison of reconnected magnetic flux and poleward expansion in the ionosphere.

proton and electron precipitation. Moving from polar cap toward lower latitudes (in the direction of convection), one first meets a very strong and energetic particle precipitation peak, indicating a strong acceleration event. The auroral precipitation (top panel of Figures 3c and S3) was enhanced in the ~ 70 -km-wide area below 73° AACG latitude, with the 130-mW/m^2 peak energy flux of 0.05- to 20-keV electrons. This region should correspond to the well-known bright poleward edge of the expanding auroral bulge (Akasofu, 1976). Comparison to Figure 3a assures that it is located at the poleward edge of westward electrojet. Here the fluxes of energetic protons and electrons also increased dramatically by 3–4 orders of magnitude above their presubstorm plasma sheet level (not shown here). The peak values were as high as $2 \cdot 10^6$ ($\text{cm}^2 \text{ s st}^{-1}$) for >30 -keV electrons and $7 \cdot 10^4$ ($\text{cm}^2 \text{ s st}^{-1}$) for >100 -keV electrons (with steep spectrum $\sim E^{-2.8}$). Strong acceleration was evident up to energies >300 keV (Figure S3). The fluxes of trapped (I_{90}) electrons and of those precipitated in the loss-cone (I_0 , red lines) are nearly equal in the 1° -wide poleward region of energetic precipitation at the transition from plasma sheet to polar cap (in the proximity of XNL), as marked by the red horizontal strip in Figures 3c and S3. Nearly isotropic loss cone electron precipitation observed in the wide energy range indicates that either B_z is small (<5 nT for standard current sheet densities) or current density is well above the norm (see, e.g., Sergeev et al., 2018, for recent application of this method) to allow the electron to undergo strong (nonadiabatic) pitch-angle scatter in the curved magnetic field during one neutral sheet crossing. Such conditions are what we expect in some area surrounding the active XNL.

Moving to even lower latitudes, we see an extended region with high energetic particle flux in the plasma sheet domain, which merges with the outer radiation belt without showing any distinct border. Since strong nonadiabatic scatter, when acting, is superior to Fermi/betatron acceleration in forming isotropic loss cone particle distribution on gyrotimescale, the systematically empty loss-cone distributions, especially pronounced for 100-keV electrons before 1947:10 UT (blue curve at the bottom), indicate ineffective nonadiabatic scatter, which occurs on the dipolarized magnetic field lines. The dipolarized region (gray strip marked as DIP in Figure 3c) spans about 7 – 8° latitude between its outer boundary at $\sim 71.8^\circ$ AACG latitude and the proton isotropy boundary IBp (at 64° AACG latitude, corresponding to the equatorial region where $B \sim 50$ nT in the inner magnetosphere, Figure S3). This is an image of extended dipolarized plasma sheet earthward of the near-Earth XNL, which is fed by reconnection outflows carrying inward the accelerated energetic particles.

3. Concluding Remarks

To our knowledge this is the first observation of relatively long (11 min) intense reconnection surge event in the magnetotail with a well-controlled reconnection rate. During the surge, the XNL seemed to stay in the same area, presumably being a few R_E earthward of MMS, close to the $X \sim -18 R_E$ distance where the XNL is often observed in the thin current sheet according to a statistical study of Cluster data (Petrukovich et al., 2009). Moreover, during the 11-min long surge observation, the MMS made measurements in the lobe near the separatrix, a highly favorable location to monitor the intense reconnection inflow and establish a lobe reconnection. Under the lobe Alfvénic field $E_A = 31$ mV/m (for $BL = 20$ nT and $N = 0.08$ cm⁻³), during the main surge the magnetic flux inflow rate of 3–6 mV/m corresponds to the 10–20% reconnection rate (E_y/E_A) which is a commonly adopted estimate found in the simulations of fast reconnection (e.g., Hesse et al., 2018). During the E_y surge the lobe magnetic field at MMS decreased by as much as ~30%, which is a very rare case, indicating a strong local loss of the lobe magnetic flux.

During this episode, the MMS did not enter the plasma sheet but crossed the separatrix a few times. Each crossing of the e-beam, directed toward the XNL, brought MMS into the region of intense E and B perturbations with $\delta E_z > 0$ ($\delta V_{E_y} < 0$) and $\delta B_y > 0$, whose polarization correspond to Hall field signatures, as expected at the location tailward and below the XNL. As expected, the Hall E_z component was significantly more intense than E_y ; the anticorrelation between $\delta \mathbf{V}E$ and $\delta \mathbf{B}$ was high and consistent with a Walén relationship. The Poynting flux was directed tailward and could reach values as large as 10^{-4} W/m², consistent with statistical results in Figure 2t from Eastwood et al. (2013). Also, at the separatrix we observed strong E -field spikes resulting both from the LH-waves and e-holes. Such structures, with amplitudes an order of magnitude larger than the reconnection electric field, are expected in this region due to the instabilities related to electron counterstreaming, as recently discussed by Hesse et al. (2016). The manifestations observed at the separatrix during the reconnection surge look quite typical for this region; however, the energy of e-beams directed toward the XNL (up to 8–10 keV) looks a bit higher than in the previous reports (few kiloelectron volts in Nagai et al., 2001) which can be attributed to the large intensity of reconnection.

Poleward auroral expansion in the nightside auroral oval during substorms is usually cited as one of the most spectacular manifestations of reconnection in the magnetotail (Hones, 1984; Baker et al., 1996, etc). However, no similar large-scale expansion is observed during steady convection events when the reconnection is also active in the magnetotail (e.g., Sergeev et al., 1996). Distinct poleward expansion of the westward electrojet was observed, in our case, exactly during the first half of reconnection surge in which the reconnection was most intense (compare Figures 1d and 3a). It allows for quantitative estimates to shed light on this apparent contradiction, including why poleward expansion is observed during some portions of substorms, but not during the steady convection events. During reconnection (see a schematic in Figure 3d), the ionospheric foot point of active XNL will move poleward in case of a stationary ambient magnetic configuration and stationary plasma sheet. Between times t_1 and t_2 , the XNL foot point will expand by a distance ΔX_i along the meridian and delineate the magnetic flux per azimuthal distance ΔY_i equal to $B_i \Delta X_i \Delta Y_i$. This quantity should be equal to the reconnected flux $E_y \Delta Y_m \Delta t$. By equating these fluxes, we obtain the poleward expansion magnitude as $\Delta X_i = E_y \Delta t (\Delta Y_m / \Delta Y_i) / B_i$. There is also an earthward convection in the plasma sheet and equatorward convection in the ionosphere. For a numerical estimate, from the TA15 model we computed the azimuthal mapping factor ($\Delta Y_m / \Delta Y_i$) to be ~40, take $B_i = 5.5 \cdot 10^4$ nT, express time in minutes, and with these values we have numerically

$$\Delta X_i \text{ (km)} \approx (44 E_y \text{ [mV/m]} - 60 V_i \text{ [km/s]}) \Delta t \text{ (min)} \quad (1)$$

Here the second term in the brackets is added to account for the equatorward ionospheric convection, V_i . Its values inside the active bulge are hard to observe by the radars because of strong radiowave absorption caused by the intense energetic electron precipitation into the D region of the ionosphere (Figure 3c). The V_i values measured by the Incoherent Scatter Radar (ISR) during a few substorms were about 0.6 km/s (de la Beaujardiere et al., 1991). Another estimate came from equatorward drift speed of auroral arcs; during substorm expansions they are typically about 0.4–0.5 km/s in the poleward part of the auroral bulge for both small and strong substorms (Kornilova et al., 1997; Figure 4). According to (1), the reconnection rate of $E_y \sim 1$ mV/m contributes about 45 km per minute to the poleward expansion, and convection

shifts the foot point back by ~ 30 km per minute if $V_i = 0.5$ km/s. This shows that a nearly stationary poleward boundary will occur if the average reconnection rate is slow, $E_Y < 1$ mV/m. In our case, the average reconnection rate between 1942 and 1947 UT was $\langle E_Y \rangle = 3.3$ mV/m, so the expected poleward expansion between 1943 and 1948 (taken with 1 min propagation time delay and suggesting the equatorward convection $V_i = 0.5$ km/s) will be 580 km, in agreement with observed poleward expansion of $\sim 6^\circ$ Lat in Figure 3a. Although not a precise estimation, this numerical agreement emphasizes an important role of the lobe reconnection in the near-Earth plasma sheet (where the lobe reconnection rate can be that high) to provide large and rapid poleward expansion in the ionosphere. This is at variance with previous interpretations linking fast large-scale poleward expansion with the tailward retreat of the XNL (Baker et al., 1996; Hones, 1984; Pytte et al., 1978).

Metop-2 passed through the expanding bulge after 1944 and crossed its polar border at 1947.5 UT, just at the minute of maximal expansion. This is a unique coincidence which results in three important conclusions.

- Comparing Figures 3a and 3c, a spectacular intense precipitation structure at the polar cap boundary (with total precipitated energy flux of 0.05–20 keV electrons exceeding 100 mW/m^2) is nearly collocated with the poleward boundary of westward AEJ. This bright precipitation at the poleward edge of the bulge is observed at the expected location of the XNL foot point; this correspondence was predicted by the NENL scenario, but now this has been observationally confirmed.
- The integral flux spectrum of energetic electrons ($E_e \sim 30\text{--}300$ keV) at the peak of this structure is rather hard ($I \sim E_e^{-2.8}$) indicating a highly efficient electron acceleration in the XNL-proximity. Here the precipitated energetic electron fluxes are as high as the fluxes observed at low altitudes in the radiation belt. Isotropic loss cone precipitation of electrons (suggesting small B_Z^2/j values in the current sheet; Sergeev et al., 2018) indicates that this may not be related to the magnetic flux pileup acceleration discussed by Hoshino et al. (2001) but rather characterizes acceleration in the outflow region adjacent to XNL. Certainly these observations reaffirm the lobe reconnection as an efficient accelerator.
- The NENL scenario predicts that reconnection outflow on the earthward side of XNL forms the dipolarized flux tubes with enhanced B_Z component and decreased current density. Most impressively, the accumulation of closed dipolarized plasma tubes ejected from XNL was illustrated in the global MHD simulations (Birn & Hesse, 2013; Wiltberger et al., 2015, etc). Here, for the first time, we show that all magnetic tubes inside the expanding auroral bulge are dipolarized as suggested by the empty loss cone of intense energetic electron fluxes in the large energy range, an immediate consequence of increased B_Z^2/j in the dipolarized plasma tubes. Being previously inferred from topological arguments, this association of the dipolarized region with the interior of the auroral bulge now receives a direct confirmation.

Acknowledgments

The used MMS data are obtainable via the MMS science data center at the website (<https://lasp.colorado.edu/mms/sdc/>). The POES and ACE spacecraft observations (in OMNI database) and some ground magnetograms have been made available via CDAWeb site (<http://cdaweb.gsfc.nasa.gov>). The data of world-wide INTERMAGNET magnetic observatories network were available at the website (www.intermagnet.org). The IMAGE magnetometer data and interpretation tools are available at the website (<http://www.space.fmi.fi/MIRACLE/iono.html>). We also thank Adrian Grocott for useful discussion. The work by V. A. S. and S. V. A. was supported by RSF grant 18-47-05001. R. N. and W. B. were supported by the Austrian Science Fund FWF.

References

- Akasofu, S. I. (1976). Recent progress in studies of DMSP auroral photographs. *Space Science Reviews*, 19(2), 169–215. <https://doi.org/10.1007/BF00215692>
- Baker, D. N., Jaynes, A. N., Turner, D. L., Nakamura, R., Schmid, D., Mauk, B. H., et al. (2016). A telescopic and microscopic examination of acceleration in the June 2015 geomagnetic storm: Magnetospheric Multiscale and Van Allen Probes study of substorm particle injection. *Geophysical Research Letters*, 43, 6051–6059. <https://doi.org/10.1002/2016GL069643>
- Baker, D. N., Pulkkinen, T. I., Angelopoulos, V., Baumjohann, W., & McPherron, R. L. (1996). The neutral line model of substorms: Past results and present view. *Journal of Geophysical Research*, 101(A6), 12,975–13,010. <https://doi.org/10.1029/95JA03753>
- Birn, J., & Hesse, M. (2013). The substorm current wedge in MHD simulations. *Journal of Geophysical Research: Space Physics*, 118, 3364–3376. <https://doi.org/10.1002/jgra.50187>
- Burch, J. L., Moore, T. E., Torbert, R. B., & Giles, B. L. (2015). Magnetospheric multiscale overview and science objectives. *Space Science Reviews*, 199(1–4), 5–21. <https://doi.org/10.1007/s11214-015-0164-9>
- De la Beaujardiere, O., Lyons, L. R., & Friis-Christensen, E. (1991). Sondrestrom radar measurements of the reconnection electric field. *Journal of Geophysical Research*, 96(A8), 13,907–13,912. <https://doi.org/10.1029/91JA01174>
- Eastwood, J. P., Phan, T. D., Drake, J. F., Shay, M. A., Borg, A. L., Lavraud, B., & Taylor, M. G. G. J. T. (2013). Energy partition in magnetic reconnection in Earth's magnetotail. *Physical Review Letters*, 110(22). <https://doi.org/10.1103/PhysRevLett.110.225001>
- Gordeev, E., Sergeev, V., Tsyganenko, N., Kuznetsova, M., Rastatter, L., Raeder, J., et al. (2017). The substorm cycle as reproduced by global MHD models. *Space Weather*, 15, 131–149. <https://doi.org/10.1002/2016SW001495>
- Hesse, M., Norgren, C., Tenfjord, P., Burch, J. L., Liu, Y.-H., Chen, L.-J., et al. (2018). On the role of separatrix instabilities in heating the reconnection outflow region. *Physics Plasmas*, 25(12). <https://doi.org/10.1063/1.5054100>
- Hesse, M., Aunai, N., Birn, J., Cassak, P., Denton, R. E., Drake, J. F., et al. (2016). Theory and Modeling for the Magnetospheric Multiscale Mission. *Space Science Reviews*, 199(1–14), 577–630. <https://doi.org/10.1007/s11214-014-0078-y>
- Hones, E. W. Jr. (1984). Plasma sheet behavior during substorms. In E. W. Hones, Jr. (Ed.), *Magnetic Reconnection in Space and Laboratory Plasmas*, Geophysical Monograph Series (Vol. 30, pp. 178–184). Washington, DC: American Geophysical Union.

- Hoshino, M., Mukai, T., Terasawa, T., & Shinohara, I. (2001). Suprathermal electron acceleration in magnetic reconnection. *Journal of Geophysical Research*, *106*(A11), 25,979–25,997. <https://doi.org/10.1029/2001JA900052>
- Kornilova, T. A., Kornilov, I. A., Pudovkin, M. I., & Starkov, G. V. (1997). Auroral arc velocities and electric field distribution during the active phase of substorms. *Geomagn/Aeronomy (Russian)*, *37*, N6, p.47-55.
- Nagai, T., Shinohara, I., Fujimoto, M., Hoshino, M., Saito, Y., Machida, S., & Mukai, T. (2001). Geotail observations of the Hall current system: Evidence of magnetic reconnection in the magnetotail. *Journal of Geophysical Research*, *106*(A11), 25929–25949. <https://doi.org/10.1029/2001JA900038>
- Paschmann, G., Øieroset, M., & Phan, T. (2013). In-situ observations of reconnection in space. *Space Science Reviews*, *178*(2-4), 385–417. <https://doi.org/10.1007/s11214-012-9957-2>
- Pembroke, A., Toffoletto, F., Sazykin, S., Wiltberger, M., Lyon, J., Merkin, V., & Schmitt, P. (2012). Initial results from a dynamic coupled magnetosphere-ionosphere-ring current model. *Journal of Geophysical Research*, *117*, A02211. <https://doi.org/10.1029/2011JA016979>
- Petrukovich, A. A., Baumjohann, W., Nakamura, R., & Rème, H. (2009). Tailward and earthward flow onsets observed by Cluster in a thin current sheet. *Journal of Geophysical Research*, *114*, A09203. <https://doi.org/10.1029/2009JA014064>
- Pytte, T., McPherron, R. L., Kivelson, M. G., West, H. I. Jr., & Hones, E. W. Jr. (1978). Multiple-satellite studies of magnetospheric substorms: Plasma sheet recovery and the poleward leap of auroral zone activity. *Journal of Geophysical Research*, *83*(A11), 5256. <https://doi.org/10.1029/JA083iA11p05256>
- Sergeev, V. A., Gordeev, E. I., Merkin, V. G., & Sitnov, M. I. (2018). Does a local B-minimum appear in the tail current sheet during a substorm growth phase? *Geophysical Research Letters*, *45*, 2566–2573. <https://doi.org/10.1002/2018GL077183>
- Sergeev, V. A., Pellinen, R. J., & Pulkkinen, T. I. (1996). Steady magnetospheric convection: A review of recent results. *Space Science Reviews*, *75*(3-4), 551–604. <https://doi.org/10.1007/BF00833344>
- Varsani, A., Nakamura, R., Sergeev, V. A., Baumjohann, W., Owen, C. J., Petrukovich, A. A., et al. (2017). Simultaneous remote observations of intense reconnection effects by DMSP and MMS spacecraft during a storm time substorm. *Journal of Geophysical Research: Space Physics*, *122*, 10,891–10,909. <https://doi.org/10.1002/2017JA024547>
- Wiltberger, M., Merkin, V., Lyon, J. G., & Ohtani, S. (2015). High-resolution global magnetohydrodynamic simulation of bursty bulk flows. *Journal of Geophysical Research: Space Physics*, *120*, 4555–4566. <https://doi.org/10.1002/2015JA021080>

References From the Supporting Information

- Tsyganenko, N. A., & Andreeva, V. A. (2015). A forecasting model of the magnetosphere driven by an optimal solar-wind coupling function. *Journal of Geophysical Research: Space Physics*, *120*, 8401–8425. <https://doi.org/10.1002/2015JA021641>